Interplay between magnetism and energetics in Fe-Cr alloys from a predictive noncollinear magnetic tight-binding model

R Soulairol, Cyrille Barreteau, Chu-Chun Fu

Interplay between magnetism and energetics in Fe-Cr alloys from a predictive noncollinear magnetic tight-binding model

R. Soulairol,[1] C. Barreteau,[2,3] and Chu-Chun Fu[1]

[1]*DEN-Service de Recherches de Métallurgie Physique, CEA, Université Paris-Saclay, F-91191 Gif-sur-Yvette, France*

[2]*SPEC, CEA, CNRS, Université Paris-Saclay, CEA Saclay 91191 Gif sur Yvette, France*

[3]*DTU NANOTECH, Technical University of Denmark, Ørsteds Plads 344, DK-2800 Kgs. Lyngby, Denmark*

(Received 16 March 2016; revised manuscript received 2 June 2016; published 21 July 2016)

Magnetism is a key driving force controlling several thermodynamic and kinetic properties of Fe-Cr systems. We present a tight-binding model for Fe-Cr, where magnetism is treated beyond the usual collinear approximation. A major advantage of this model consists in a rather simple fitting procedure. In particular, no specific property of the binary system is explicitly required in the fitting database. The present model is proved to be accurate and highly transferable for electronic, magnetic, and energetic properties of a large variety of structural and chemical environments: surfaces, interfaces, embedded clusters, and the whole compositional range of the binary alloy. The occurrence of noncollinear magnetic configurations caused by magnetic frustrations is successfully predicted. The present tight-binding approach can apply to other binary magnetic transition-metal alloys. It is expected to be particularly promising if the size difference between the alloying elements is rather small and the electronic properties prevail.

DOI: 10.1103/PhysRevB.94.024427

I. INTRODUCTION

Iron-chromium systems have triggered extensive research efforts during the last few decades. On one side, it is due to their complex magnetostructural interplay, including the emergence of noncollinear magnetic configurations in the vicinity of structural defects and chemical heterogeneities [1,2]. Magnetic interactions and frustrations are also shown to dictate thermodynamic properties such as the well-known atypical mixing-enthalpy behavior of the Fe-Cr alloy. Electronic-structure-based modeling by Hennion [3] in 1983, confirmed later by experimental neutron studies of chemical short-range order (SRO) [4,5], has shown that Fe-Cr alloys with a low-Cr content (in a ferromagnetic state) display an ordering tendency while they exhibit a tendency to phase separation at higher Cr concentrations. The experimental crossover Cr concentration was found to be around 11% [5]. Recently, this anomaly has been extensively investigated via various *ab initio* methods [6–11]. Consistent with the experimental evidence, all the studies agree on the sign change of the mixing enthalpy in the ferromagnetic phase, although the crossover depends on the approach, varying from 5% to around 15% of Cr. Some of these works [6,7,9,10] also showed that this anomaly disappears if considering magnetically disordered systems which represent the high-temperature paramagnetic Fe-Cr alloys.

On the other side, the studies on Fe-Cr systems are motivated by their relevance for a large variety of technological applications. For instance, ferrito-martensitic steels with a high-Cr content (around 10% Cr) show improved resistance to corrosion, irradiation, and swelling. They are therefore promising materials for innovative nuclear devices. Also, Fe/Cr multilayers were at the origin of the discovery of giant magnetoresistance [12,13] which rapidly lead to tremendous applications in electronic devices.

Numerous atomic-scale studies based on density functional theory (DFT) have pointed out a strong correlation between magnetic and energetic properties in the Fe-Cr alloys [8,14–17]. In the body-centered-cubic (bcc) lattice, local magnetic moments on Fe atoms tend to be parallel (ferromagnetic), local moments on first-nearest-neighbor (1NN) Cr atoms tend to be antiparallel (antiferromagnetic), and within a simplified picture, moments of 1NN and second-nearest-neighbor (2NN) Fe-Cr pairs prefer to be antiparallel [2,8]. Magnetic frustrations occur when these magnetic tendencies cannot be satisfied simultaneously. As a consequence, noncollinear magnetic configurations and/or spin waves emerge in order to resolve partially the frustrations. This happens around the interfaces of Fe-Cr multilayers and of small clusters and precipitates in the binary alloy [1,2,18]. Also, experiments and simulations indicated a mutual dependence of the microstructure and the global magnetization of the alloy [18,19]. In addition, the kinetics of phase decomposition in rather concentrated Fe-Cr alloys were shown to be very sensitive to the magnetic state of the system [20,21].

Based on the above-mentioned evidences, an accurate description of the electronic structure and magnetism is essential for a reliable prediction of the thermodynamic, kinetic, and defect and microstructural properties of the Fe-Cr alloys. Aside from the first-principles methods, semiempirical interatomic potentials and models are often required for performing atomistic studies on systems containing defects (nanoclusters, dislocations, grain boundaries, etc.), where large supercells, not reachable with DFT, should be adopted. In the case of Fe-Cr, empirical potentials based on the embedded atom model have been developed [22–24], where magnetic effects are taken into account only implicitly through the input parameters. It is not obvious that these potentials are able to predict the complex interplay between magnetism and energetic and structural properties of the defects. Tight-binding (TB) models offer a promising alternative, where the electronic structure and magnetism are explicitly considered. Previously, TB modeling of Fe/Cr interfaces were performed, addressing mainly the magnetic behavior [25–28]. More recently, a few tight-binding models were developed paying special attention on the energetics and thermodynamics of Fe-Cr alloys [29–31]. Attempting to go beyond, we present a TB model, capable

to predict both energetic and magnetic properties in the defect-free Fe-Cr alloys of different chemical compositions and ordering, and in the vicinity of surfaces, interfaces, and nanoclusters. One specificity of this TB model is that no property from the binary system is explicitly included in the fitting data. In addition, the magnetism is treated beyond the usual collinear approximation, which is crucial for an accurate description of the Fe-Cr system.

This paper is organized as follows: The TB formalism, the parameters, and the fitting procedure are described in Secs. II A–II D. A comparison between the present and the previous TB models is given in Sec. II E. In Sec. III, we show the validity and transferability of the TB model by considering key properties of surfaces, interfaces, alloys of different compositions, the ordered B2 structure and small clusters, through a close comparison with the corresponding DFT results. Finally, conclusions are given in Sec. IV, and all the TB parameters are listed in the Appendix.

II. A MAGNETIC *spd* TIGHT-BINDING MODEL FOR ALLOYS

A. TB model for a single chemical-element system

We have developed over the years an efficient scheme based on a tight-binding model which we have extended to spin-polarized systems [32–34]. We will first recall the main ingredients of our model applied to single chemical elements and then generalize it to metallic binary alloys. The Hamiltonian is divided into three contributions:

$$H = H^{\mathrm{TB}} + V^{\mathrm{LCN}} + V^{\mathrm{Stoner}}, \tag{1}$$

where H^{TB} is the nonmagnetic TB Hamiltonian made of diagonal elements $\epsilon_{i\lambda} = \langle i,\lambda|H|i,\lambda\rangle$ and hopping integrals $\beta_{i\lambda,j\mu} = \langle i,\lambda|H|j,\mu\rangle$, where $|i,\lambda\rangle$ ($|j,\mu\rangle$) is the orbital λ (μ) on atomic site i (j). The intra-atomic terms are written as a function of the local environment as in the work of Mehl and Papaconstantopoulos [35]:

$$\epsilon_{i\lambda} = a_\lambda + b_\lambda \rho_i^{1/3} + c_\lambda \rho_i^{2/3} + d_\lambda \rho_i^{4/3} + e_\lambda \rho_i^2. \tag{2}$$

$a_\lambda, b_\lambda, c_\lambda, d_\lambda$, and e_λ are parameters to determine. Note that the expression (2) differs from that of Ref. [35] since it contains an additional term $\rho_i^{1/3}$ which gives supplementary flexibility and improves significantly the quality of the fit to *ab initio* data at large interatomic distances. ρ_i is related to the atomic density around atom i:

$$\rho_i = \sum_{j\neq i} \exp[-\Lambda^2 r_{ij}] F_c(r_{ij}), \tag{3}$$

where the sum runs over the neighboring sites j surrounding atom i, Λ is also a parameter and $F_c(r)$ a cutoff function truncating interactions for distances larger than a given radius $R_c = 16.5$ bohrs, with a Fermi-Dirac–type transition that brings the potential smoothly to zero between $R' = 14$ bohrs and R_c.

The hopping integrals $\beta_{i\lambda,j\mu}$ as well as the overlap integrals $S_{i\lambda,j\mu} = \langle i,\lambda|j,\mu\rangle$ are written in terms of 10 Slater-Koster [36] parameters $\beta_\gamma = ss\sigma, sp\sigma, sd\sigma, pp\sigma, pp\pi, pd\sigma, pd\pi, dd\sigma, dd\pi, dd\delta$ which themselves are given in an analytical form as a product of a decaying exponential and a polynome depending on several parameters:

$$\beta_\gamma(r) = (p_\gamma + f_\gamma r + g_\gamma r^2) \exp\big[-h_\gamma^2 r\big] F_c(r). \tag{4}$$

V^{LCN} is the so-called "local charge neutrality" term that avoids charge transfers by imposing a given electronic charge on each atom. The matrix elements of the corresponding potential have the following form:

$$V^{\mathrm{LCN}}_{i\lambda\sigma,j\mu\sigma'} = \tfrac{1}{2}\big[U_i\big(N_i - N_i^0\big) + U_j\big(N_j - N_j^0\big)\big] S_{i\lambda j\mu}\delta_{\sigma,\sigma'}, \tag{5}$$

where N_i (N_j) is the Mulliken charge of atom i (j) and N_i^0 (N_j^0) the charge that one wants to impose on site i (j). U_i depends only on the nature of the chemical element occupying site i and determines the "strength" of the neutrality condition. V^{LCN} is diagonal in spin space and acts indifferently on up and down spins.

Finally, V^{Stoner} is the Stoner Hamiltonian which is the simplest but physically sound way to introduce magnetism in a tight-binding scheme. Its action is to split up and down bands in the following way:

$$V^{\mathrm{Stoner}}_{i\lambda\sigma,j\mu\sigma'} = -\frac{I_{i\lambda}}{2}(M_{id}\sigma\delta_{\sigma,\sigma'})\delta_{i\lambda,j\mu}, \tag{6}$$

where $\sigma = \pm 1$ denotes the up and down spin. $I_{i\lambda}$ is the so-called Stoner parameter acting on orbital λ and site i, and M_{id} is the component of the spin magnetization of atom on site i summed over the d orbitals only. In transition metals, the d orbitals are those bearing the magnetism which value is controlled by the amplitude of I_{id} (the exact value of I_{is} and I_{ip} has a minor effect on the total magnetization but in practice we took $I_s = I_p = I_d/10$). V^{Stoner} is diagonal in the spin space and produces a shift between up and down spins.

The Stoner potential can straightforwardly be generalized to the case of noncollinear magnetism where the magnetization at each site can take any direction and must be described by a three-component vector $\boldsymbol{M}_{id}$. The potential now acts on both components of the spin orbitals and can be written as a 2×2 matrix:

$$\tilde{V}^{\mathrm{Stoner}}_{i\lambda,j\mu} = -\frac{I_{i\lambda}}{2}(\boldsymbol{M}_{id}.\boldsymbol{\sigma})\delta_{i\lambda,j\mu}. \tag{7}$$

$\boldsymbol{\sigma}$ is the vector built from the three Pauli matrices $(\sigma_x,\sigma_y,\sigma_z)$ and the tilde denotes a 2×2 matrix acting on a two-component spin orbital.

The total energy of the system is written in accordance with the work of Mehl and Papaconstantopoulos [35] as the sum of the occupied one-electron eigenvalues ε_α. This band term should, however, be corrected by the so-called double-counting terms arising from electron-electron interactions introduced by LCN correction and Stoner terms [37]. The total energy is then written as

$$E_{\mathrm{tot}} = \sum_\alpha f_\alpha \varepsilon_\alpha - \frac{1}{2}\sum_i U_i\big[N_i^2 - \big(N_i^0\big)^2\big] + \frac{1}{4}\sum_{i,\lambda} I_{i\lambda}\boldsymbol{M}_{i\lambda}.\boldsymbol{M}_{id}, \tag{8}$$

f_α being the occupation of state α. The first term of the right-hand-side expression is the so-called band energy of the

magnetic Hamiltonian given by Eq. (1) and the two other terms accounts for the double-counting corrections arising from the local charge neutrality and Stoner potential.

Note that due to the electron-electron interaction, the Hamiltonian depends on the local charges and magnetic moments and thus the diagonalization of the Hamiltonian should be carried out self-consistently until the convergence criterion on the charge (and energy) is achieved.

It is worth mentioning that in the limit of large Coulomb interactions, the term $U_i(N_i - N_i^0)$ converges towards a finite value δV_i while N_i approaches N_i^0. The double-counting correction term then takes the simple form $-\sum_i \delta V_i N_i^0$ valid in the limit of exact charge neutrality.

B. Determination of the TB parameters for single-element systems

The determination of the TB parameters is made in two steps. First, all the parameters of H^{TB} are obtained from a nonlinear mean-square fit to bulk nonmagnetic DFT calculations in the generalized gradient approximation (GGA). The fitting database consists of band structures and total energies calculated over a large range of lattice parameters (typically for interatomic distances between 2.2 and 7 Å but with a larger weight for distances around equilibrium) and three different crystallographic structures, namely, face-centered cubic (fcc), body-centered cubic (bcc), and simple cubic (sc) simultaneously. An excellent agreement between TB and DFT results is obtained for both elements in the nonmagnetic phase. Note that our fit is performed on a much larger interatomic range than in Ref. [35] since we found that it significantly improves the transferability of our model with respect to the magnetic properties. This problem stems from the fact that the magnetization curve $M(a_{\mathrm{lat}})$ (see below) is very sensitive to the asymptotic limit for large interatomic distances.

In a second step we determine the value of the Stoner parameter. This is done by a trial and error approach where one tries to reproduce as precisely as possible the evolution of the magnetic moment M of bulk materials with the lattice parameter a_{lat} obtained from spin-polarized DFT calculations. Such calculations were performed on bulk bcc ferromagnetic (FM) iron and bulk bcc antiferromagnetic (AF) chromium. We found that $I_d^{\mathrm{Cr}} = 0.82$ eV is a very good estimate for chromium while the case of iron is slightly more complex since it is difficult to reproduce the DFT results over the whole range of lattice parameters. Indeed, we found that for lattice parameters below 2.85 Å, the best value for the Stoner parameter is $I_d^{\mathrm{Fe}} = 0.88$ eV, while for lattice parameters above 2.95 Å a larger Stoner parameter ($I_d^{\mathrm{Fe}} = 0.95$ eV) describes more accurately the $M(a_{\mathrm{lat}})$ curve. In addition, the phase stability of iron is in much better agreement with *ab initio* data with $I_d^{\mathrm{Fe}} = 0.95$ eV than with $I_d^{\mathrm{Fe}} = 0.88$ eV, therefore, all the calculations in this paper were performed with $I_d^{\mathrm{Fe}} = 0.95$ eV. These values agree well with those derived from *ab initio* band structure calculations in the seminal work of Janak [38] where the author found $I^{\mathrm{Fe}} = 0.92$, $I^{\mathrm{Cr}} = 0.76$ eV (note that from Table I of Ref. [38] the values for the Stoner exchange integrals should be multiplied by two due to a different normalization factor).

C. Phase stability of Fe and Cr

Since our aim is to model Fe-Cr alloys over the whole concentration range, it is essential to correctly reproduce the phase stability of both pure elements. This is particularly challenging for Fe since it is known that even within DFT the choice of the functional can be crucial to accurately reproduce its phase stability. For instance, it is well known that within local spin density approximation (LSDA) the nonmagnetic hexagonal closed packed (hcp-NM) is found to be the most stable structure. It is only by using the generalized gradient approximation (GGA) that the most stable ferromagnetic body centered (bcc-FM) is recovered. This is why we have fitted the TB parameters on GGA, DFT data. The relative stability of magnetostructural phases can be determined from energy versus atomic volume curves as plotted in Fig. 1 for Fe and Cr. The results are in surprisingly good agreement with DFT calculations of Ref. [39]. In particular, the sequence in energy of the various phases of iron is almost perfectly reproduced. The bcc-FM is found to be the most stable at an equilibirum lattice parameter of $a_{\mathrm{bcc}}^{\mathrm{Fe}} = 2.845$ Å close to the experimental value (2.87 Å). The fcc Fe phase has a much more complex magnetoenergetic landscape with the presence of several magnetic solutions close in energy. Our calculations predict a double-layer AF configuration (AFD) to be the most stable one among all the Fe fcc phases as in DFT calculations [39,40]. For chromium, the phase-stability diagram is much simpler since the bcc lattice is strongly favored as expected from d-band filling arguments [41] and the magnetic AF structure gets only slightly lower in energy for lattice parameters above 2.84 Å. The equilibrium is found at $a_{\mathrm{bcc}}^{\mathrm{Cr}} = 2.885$ Å as compared to the experimental value of 2.91 Å.

D. TB model for Fe-Cr binary systems

If we consider now the Fe-Cr metallic alloy, the following procedure (which can be applied to any other transition-metal alloy) has been carried out. A fit for both chemical elements is performed separately with the same value of Λ. Then, the intra-atomic terms of the Hamiltonian for a given site i will only depend on the nature of the chemical species occupying site i by the value of the coefficients a_λ, b_λ, c_λ, and d_λ for the corresponding atom. The hopping and overlap integrals between two identical atoms (Fe-Fe or Cr-Cr) are the same as those obtained for the pure elements while the heteronuclear value (Fe-Cr) is taken as the arithmetic average multiplied by a small (yet important) rescaling factor $\eta_{\text{Fe-Cr}}$:

$$\beta_\gamma^{\text{Fe-Cr}}(R) = \frac{\beta_\gamma^{\mathrm{Fe}}(R) + \beta_\gamma^{\mathrm{Cr}}(R)}{2}\eta_{\text{Fe-Cr}}. \tag{9}$$

The distance dependence of the Slater-Koster d hopping and overlap integrals is illustrated in Fig. 2. As expected, the hopping (and overlap) integrals of Cr are larger than the one of Fe. In addition, they can be very well approximated by a single exponential decay but this is not the case for the integrals involving s and p orbitals (not shown in Fig. 2). The effect of $\eta_{\text{Fe-Cr}}$ is minor on the electronic and magnetic properties of the Fe-Cr alloy (magnetic moments are hardly affected by $\eta_{\text{Fe-Cr}}$) but the energetics of the alloy depend crucially on its numerical value. For example, without rescaling, the interface energies

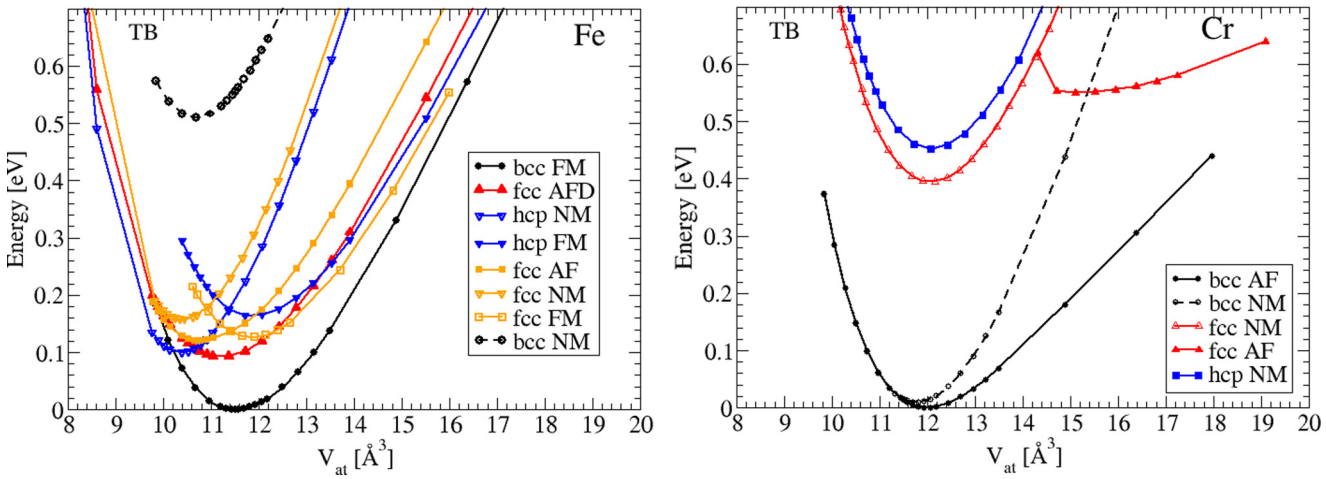

FIG. 1. Total energy (per atom) as a function of the atomic volume for various crystallographic structure [body-centered cubic (bcc), face-centered cubic (fcc), and hexagonal closed pack (hcp)] of Fe (left) and Cr (right). Several magnetic solutions are considered: nonmagnetic (NM), ferromagnetic (FM), simple-layer antiferromagnetic (AF), double-layer antiferromagnetic (AFD).

and the mixing energy of B2 phase are largely overestimated by a factor of more than 2. In addition, the specific negative feature of the mixing enthalpy curve at low-Cr concentrations can only be reproduced for η values larger than one. We found that $\eta_{\text{Fe-Cr}} = 1.023$ gives the best results.

The role of the LCN term is evidently crucial in binary alloys since it controls the charge on each atom. If the value of the Coulomb interaction U is taken large enough, the LCN condition is almost exactly fulfilled and the charge of a given atom of the system is equal to the valence charge of the corresponding element. In all this work, we took $U = 30$ eV for both elements which is sufficient to keep charge transfers as small as possible. The Stoner parameter is taken as in the pure elements $I_{i,d} = I_d^{\text{Fe}} = 0.95$ eV if site i is occupied by an iron atom and $I_{i,d} = I_d^{\text{Cr}} = 0.82$ eV if site i is occupied by a chromium atom.

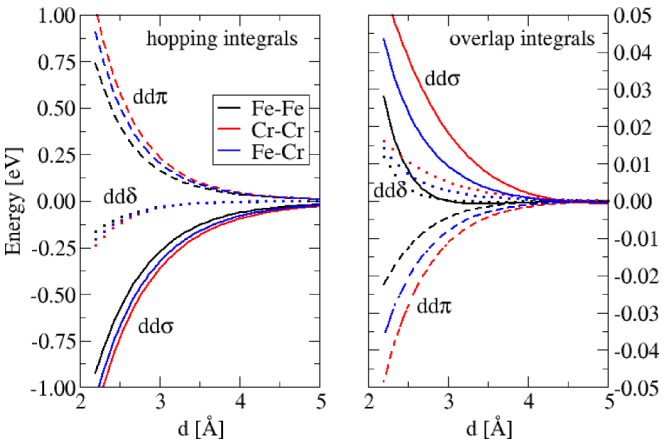

FIG. 2. Two-center Slater-Koster d hopping (left) and overlap (right) integrals as a function of the interatomic distance r between two Fe-Fe, Cr-Cr, and Fe-Cr atoms. The Fe-Cr hopping and overlap integrals are rescaled by a factor 1.023 with respect to the arithmetic average.

Finally, let us insist on the relative simplicity of our TB model for bimetallic systems since it does not require any fitting to *ab initio* data from the binary alloy. The local charge neutrality condition aligns the respective local density of states so that the Mulliken charge of each atom is close to the valence charge of the corresponding chemical species. The hopping and overlap integrals are obtained from the ones of the pure elements. The only slight adjustment is related to the scaling factor $\eta_{\text{Fe-Cr}}$ which has a crucial influence on the energetics of the alloy, but a very small influence on its electronic and magnetic structure (at least for the very modest value taken in the case of Fe-Cr: 1.023). In particular, it is necessary to reproduce accurately the negative enthalpy of mixing for low-Cr concentration of the Fe-Cr alloy. Let us also stress the generality of our procedure which can basically be applied to any alloy.

E. Comparison with existing tight-binding models

In the past, several TB modelings for Fe-Cr were performed but they were addressing mainly magnetic properties, in particular the frustration effects and noncollinear configurations at interfaces [25–28]. More recently, we are aware of essentially three magnetic tight-binding models to describe both energetic and magnetic properties of the binary Fe-Cr alloy: two are based on a d-band model [30,31] and one on a spd-band model [29]. The two d-band models are very similar apart from details like the dependence of hopping integrals with interatomic distance which is exponential in Ref. [31] or a power law in Ref. [30]. The repulsive potential is also different since in Ref. [31] an embedding potential is added to take into account the contribution of s orbitals (ignored in Ref. [30]). The advantage of pure d-band models is evidently their simplicity and also their numerical efficiency. However, one crucial parameter is the number of d electrons N_d that should be defined, and when one is dealing with magnetic systems the choice of N_d should be done concomitantly with the Stoner parameter I_d. There is evidently a rather large margin of choice since the two "parameters" are intimately connected. For example, in Ref. [30] they take $N_d = 4.4$

and $I_d = 0.7$ eV for Cr while in Ref. [31] it is $N_d = 5.4$ and $I_d = 0.54$ eV. We believe that such a large variation of important parameters will necessarily lead to rather different physical behaviors in certain conditions, meaning that their transferability needs to be checked very carefully. In addition, the electronic density of states is less faithfully reproduced than in an *spd* model and several important features are often lacking.

The *spd*-band model of Ref. [29] is much closer to our model since not only it includes explicitly all the valence electrons, but also takes into account overlap integrals. The two *spd* models essentially differ by two aspects: the distance dependence of their hopping and overlap integrals is simpler (exponential) than ours and the total energy is written as a sum of band and repulsive energy while we have adopted the procedure proposed by Mehl and Papaconstantopoulos [35] where the total energy (of a nonmagnetic system) is written as the band energy only but onsite levels are varying with the local environment via Eq. (2).

The specificity of our model is that we have fitted the hopping and overlap integral parameters to describe as closely as possible the band structure and total energies of pure elements obtained from *ab initio* calculations on several crystallographic structures and over a large range of interatomic distances. We found this procedure important to reproduce accurately the complex intertwined magnetic and structural properties of Fe and Cr. For example, our model perfectly reproduces the complex phase stability diagram in iron (see Fig. 1) which is not possible with the simpler model of Ref. [29] and consequently it is not possible to study the mixing energies. In fact, in the work of Paxton *et al.* the authors essentially focus on the magnetic contribution (Stoner type) to the total energy but not on the chemical contribution.

Our TB scheme has also been tested extensively to calculate magnetocrystalline anisotropy (therefore including spin-orbit coupling) in iron and cobalt with excellent quantitative agreement with *ab initio* methods [42,43]. Concerning the Fe-Cr alloy, we have adopted a simple and straightforward procedure which proved to be very efficient and accurate.

III. MODEL VALIDATION AND RESULTS

Before discussing our results, let us mention that in all our calculations we have only considered the standard antiferromagnetic (AF) configuration of bcc chromium and ignored any effect due to the spin-density wave (SDW) which is the true ground state of the material. We believe that the neglect of the SDW order has a modest influence on the following results since SDW and AF are very close energetically [39] and it is known experimentally that the SDW phase disappears (in favor of the AF) above a few percent of Fe incorporated in Cr. In addition, structural relaxations are ignored.

In the following, we compare systematically the surface energies of pure systems and various properties of the Fe-Cr alloys resulting from this TB model and predicted by our previous DFT studies [1,11,18]. The DFT calculations were performed using the SIESTA code [44] within GGA in the Perdew-Burke-Ernzerhof (PBE) form. Core electrons are replaced by nonlocal norm-conserving pseudopotentials, while valence electrons are described by a linear combination of numerical pseudoatomic orbitals (LCAO). Either collinear or noncollinear treatment of magnetism has been adopted. A detailed description of the DFT simulation setup can be found in Refs. [1,11,18]. We have chosen to compare the TB with the DFT-SIESTA results because the use of LCAO type of basis sets makes SIESTA more "similar" to the TB scheme than the plane-wave DFT methods.

A. Surfaces

Before discussing the case of binary systems, let us first consider the two lowest-index (001) and (110) surfaces of the pure elements. The surfaces are modeled by slabs of 27 atomic layers. Each atomic layer contains one atom per unit cell in the case of the (001) orientation and two atoms in the case of (110). Therefore, the slab of (110) orientation contains twice more atoms N^{at} than the one of (001) orientation. In the case of iron, the two atoms are equivalent and bear the same spin moment, while for chromium they have opposite magnetic moments. Structural relaxations are ignored and the lattice parameters are fixed to their respective bulk equilibrium values $a_{\text{bcc}}^{\text{Fe}} = 2.845$ Å for Fe and $a_{\text{bcc}}^{\text{Cr}} = 2.885$ Å for Cr. The surface energies per surface area are calculated by the usual formula

$$E^{\text{surf}} = \frac{1}{2A}[E^{\text{tot}}(\text{slab}, N^{\text{at}}) - N^{\text{at}} E^{\text{tot}}(\text{bulk})], \qquad (10)$$

where A is the area of the surface unit cell. $E^{\text{tot}}(\text{slab}, N^{\text{at}})$ and $E^{\text{tot}}(\text{bulk})$ denote the total energy of the slab (containing N^{at} atoms) and of the bulk, respectively. The numerical values are presented in Table I.

The magnetization is usually enhanced at surfaces as illustrated by Figs. 3 and 4 showing the evolution of the spin

TABLE I. Unrelaxed surface energies per surface atom and per surface area for the (001) and (110) crystallographic orientations of bcc iron and chromium. Values within parentheses are the relaxed surface energies. Note that the surface energy (per surface area) of the (001) orientation is lower than that of the (110) orientation in the case of chromium. This is attributed to a very large enhancement of the magnetization on the outermost layer of bcc Cr(001).

Surface	eV/atom	J/m^2	eV/atom	J/m^2	J/m^2	
Method	TB		DFT-SIESTA		DFT [45,46]	DFT [47]
Cr(001)	1.606	3.091	1.75	3.38 (3.37)	(3.25) [46]	(3.00)
Fe(001)	1.229	2.433	1.47	2.87 (2.85)	2.48 (2.47) [45]	(2.50)
Cr(110)	1.157	3.150	1.26	3.44 (3.44)		(3.10)
Fe(110)	0.750	2.100	0.99	2.70 (2.70)	2.38 (2.37) [45]	(2.45)

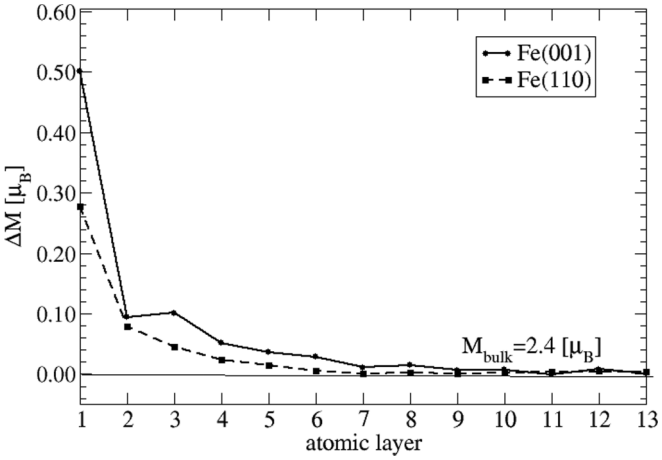

FIG. 3. Variation of the excess spin magnetization per atom (with respect to the bulk value) decomposed on successive atomic layers for the (001) and (110) surfaces of Fe.

moment as penetrating into the bulk of the material from its surface. This magnetization enhancement has consequences on their energetics and can even modify the general trend for the surface energies. Previous theoretical works have already pointed out an anomalous surface energy behavior of 3*d* metals as a function of the *d*-band filling, deviating from the simple parabolic trend. Specific properties of surfaces of the magnetic 3*d* elements (Cr, M, Fe, Co) were identified to explain the behavior [47–49]. The surface energies of nonmagnetic transition metals follow the rule of thumb based on the number of broken bonds that the densest surfaces have the lowest surface energies. However, the surface magnetization follows an opposite rule that favors less dense surfaces since the more neighbors are lost at the surface, the more the magnetization is increased with respect to the bulk. As a consequence, less dense surfaces lower their energies by increasing their magnetization. In the case of chromium (001) the strong enhancement of the surface magnetization $\Delta|M_{\text{surf}}| = |M_{\text{surf}}| - |M_{\text{bulk}}| = 2\mu_B$ is

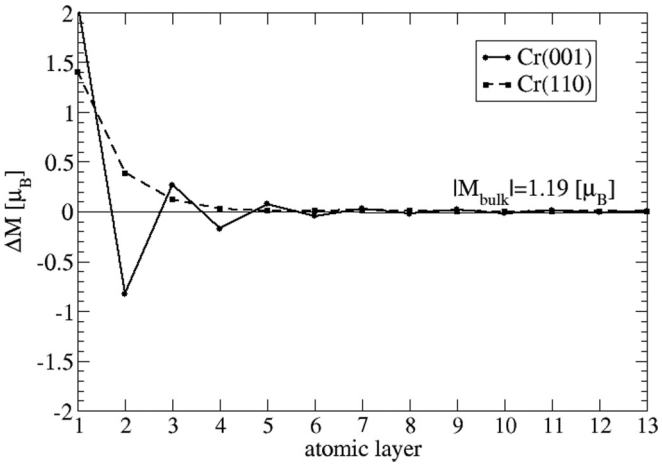

FIG. 4. Variation of the excess spin magnetization per atom (with respect to the bulk value) decomposed on successive atomic layers for the (001) and (110) surfaces of Cr. Note the particularly strong enhancement of magnetization at the outermost layer of Cr(001).

strongly stabilizing this surface which energy (per surface area) is lower than the (110) surface energy. The surface energies and in particular the energy difference between these two crystallographic orientations for both Fe and Cr are in overall good agreement with various DFT results (Table I). We note an overestimation of the surface energy anisotropy ratio ($E^{\text{surf}}_{(001)}/E^{\text{surf}}_{(110)}$) between Fe(001) and Fe(110) from the TB model (1.16), compared with the DFT estimations (1.06 from SIESTA, 1.04 from Ref. [45], and 1.02 from Ref. [47]). This is due to a slight underestimation of the difference of surface magnetization between the Fe(100) and Fe(110) by the TB model. This value is $0.22\mu_B$ per surface atom from the TB, and around 0.3 to $0.36\mu_B$ from the DFT studies. However, the anisotropy ratio between the Cr(110) and the Cr(001) surfaces is accurately reproduced by the TB model (1.019 from TB and 1.018 from SIESTA). Note also that there is only a tiny effect of atomic relaxations on the surface energies (Table I).

B. Fe/Cr interfaces

Let us now consider an interface between iron and chromium and investigate the role of magnetism on the energetics. Some diffuse interfaces between some Fe and Cr alloys have been considered by previous DFT studies [50]. Here, for simplicity, we consider only the abrupt interfaces between pure Fe and Cr phases. Regarding the magnetic properties, the (001) and (110) interfaces are expected to behave very differently since a strong frustration is present at the (110) interface due to the impossibility to fulfill the first-neighbor antiferromagnetic coupling between Fe and Cr while at the (001) interface such frustration does not exist (at least for the first-neighbor interactions). The systems are modeled by sticking together 27 layers of Fe and 27 layers of Cr. The lattice parameter is taken as the average value $a^{\text{int}} = \frac{1}{2}(a^{\text{Fe}}_{\text{bcc}} + a^{\text{Cr}}_{\text{bcc}}) = 2.865$ Å and structural relaxations are ignored. The unit cell therefore contains 54 atoms in the case of the (001) interface and twice more for the (110) interface. Collinear and noncollinear magnetic configurations are considered. For noncollinear structures, the starting magnetization is essential. We chose the initial magnetic moment of iron and chromium atoms to be perpendicular and let the system evolve until convergence was achieved. In the case of the (001) interface, the final configuration is the collinear one (Fig. 5) while for the (110) a noncollinear magnetic solution does exist for which iron and chromium atoms away from the interface have perpendicular magnetization, while a small canting of the spin moments is observed in the vicinity of the interface (Fig. 6).

The formation energy (per unit interface area) of a given interface is then obtained from the formula

$$E^{\text{int}} = \frac{1}{2A}[E^{\text{tot}}(\text{int}, N^{\text{Fe}}/N^{\text{Cr}}) - N^{\text{Fe}}E^{\text{Fe, tot}}(\text{bulk}) - N^{\text{Cr}}E^{\text{Cr, tot}}(\text{bulk})], \quad (11)$$

where $E^{\text{tot}}(\text{int}, N^{\text{Fe}}/N^{\text{Cr}})$ is the total energy of the unit cell containing N^{Fe} iron atoms and N^{Cr} chromium atoms. $E^{\text{Fe, tot}}(\text{bulk})$ and $E^{\text{Cr, tot}}(\text{bulk})$ are the respective bulk energy (per atom) of iron and chromium. The factor $2A$ accounts for the presence of two identical interfaces per unit cell. The results are summarized in Table II.

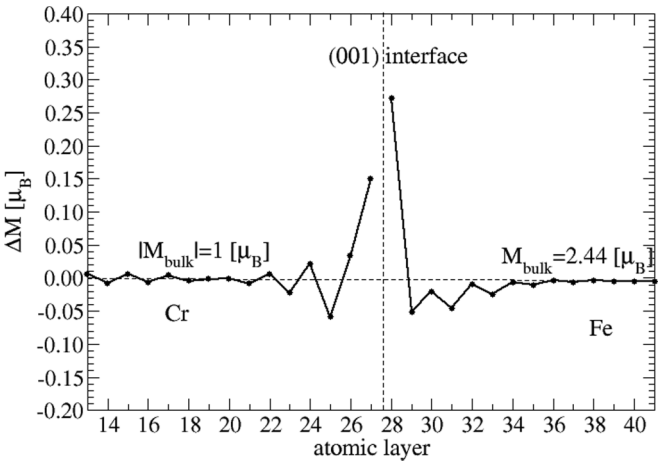

FIG. 5. Excess local moments with respect to the corresponding bulk value ($M^{\text{bulk,Cr}} = \pm 1\mu_B$ and $M^{\text{bulk,Fe}} = 2.44\mu_B$) across the Fe-Cr (001) interface.

The obtained noncollinear ground-state structure for the (110) interface as well as the various interfaces energies from TB are in excellent agreement with DFT data. The lowest formation energy is obtained for the (001) interface which can be attributed to two concomitant mechanisms: (i) a stabilization of the (001) interface due to an enhancement of the magnetization at the interface and (ii) a strong frustration effect

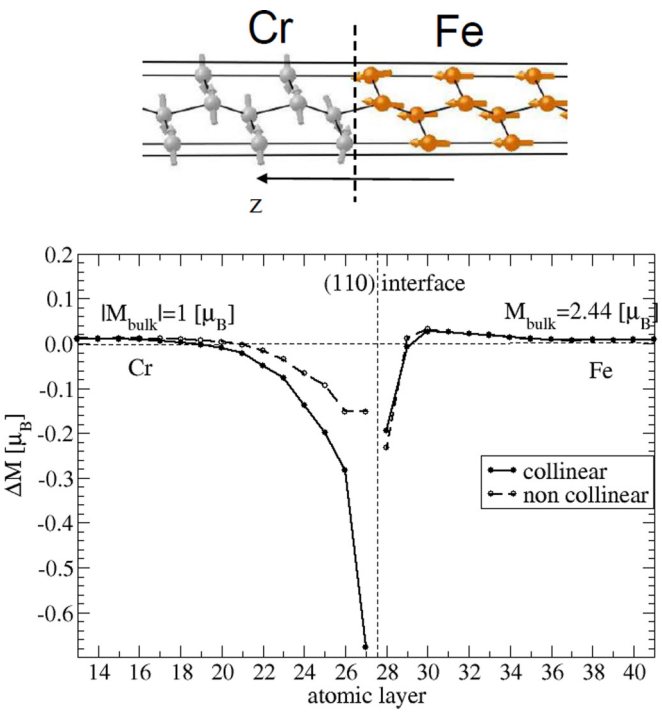

FIG. 6. Top: noncollinear magnetic configuration in the vicinity of the Fe-Cr (110) interface. Bottom: excess local moments with respect to the corresponding bulk value ($M^{\text{bulk,Cr}} = \pm 1\mu_B$ and $M^{\text{bulk,Fe}} = 2.44\mu_B$) across the Fe-Cr (110) interface for a collinear and and noncollinear magnetic solution. We note a rather modest canting of the magnetic moments of chromium and iron in the vicinity of the interface.

TABLE II. Unrelaxed interface energy per interface atom and per interface area between Fe and Cr for the (001) and (110) crystallographic orientations. Collinear and noncollinear magnetic structures are presented. Note that in the case of the (001) interface, all noncollinear initial configurations converge towards the most stable collinear configuration.

Surface	eV/atom	J/m^2	eV/atom	J/m^2
Method	TB		DFT-SIESTA [1]	
(001) collinear	0.058	0.114	0.062	0.120
(110) collinear	0.065	0.180	0.073	0.200
(110) noncollinear	0.055	0.150	0.069	0.190

in play at the (110) interface that decreases the amplitude of the magnetization at the interface and consequently penalizes the energetics of this interface. This frustration can be partly released by the development of a noncollinear magnetic configuration in the vicinity of the interface.

The present TB prediction of the interfacial energy anisotropy in the collinear case with the AF state for Cr is also consistent with a previous DFT data evaluating the adhesion energies of the same abrupt (100) and (110) Fe/Cr interfaces [51]. On the other side, the energies seem to differ from the case with very few Fe and Cr layers, where residual interaction may exist between the two interfaces in the same simulation cell. For instance, Lu *et al.* [50] found a slightly higher interface energy for the (100) than for the (110), when considering relatively small supercells, i.e., with no more than five atomic layers of each element.

C. B2 phase

The simplest ordered crystallographic structure of the equiatomic Fe-Cr alloy is the B2 (or Cs-Cl) structure. The crystal system is simple cubic with two atoms per unit cell based on the bcc lattice where one atomic species occupies the corner of the cube and the other the center. This B2 phase has a very high formation energy in the case of Fe-Cr, but it is worth studying from the magnetic point of view. Indeed, although its crystallography is very simple, the magnetic structure of Fe-Cr B2 is rather complex and several nontrivial solutions do exist in this phase. Inspired by the work of Qiu *et al.* [52], we have considered not only the B2 two-atom unit cell, but also the four-atom magnetic unit cell (see Fig. 7) built from two adjacent cubes in the (001) direction. We have performed a careful investigation of the various magnetic structures by scanning many different initial magnetizations for the four (magnetically) inequivalent atoms in the unit cell. We have finally identified four different solutions (plus the nonmagnetic one) in a given range of lattice parameters. Two of them (AFS and FM/AF) can be described by the elementary B2 unit cell and the two others (AF-FMD and AFD) require the double four-atom unit cell. Once these four solutions have been identified, we have been able to study their evolution with the lattice parameter in a range of lattice parameters around the equilibrium distance. In practice, it was made possible to "follow" these solutions by performing a series of calculations on a fine grid of lattice parameters starting from input charges and magnetization obtained from a previous solution. In Fig. 7,

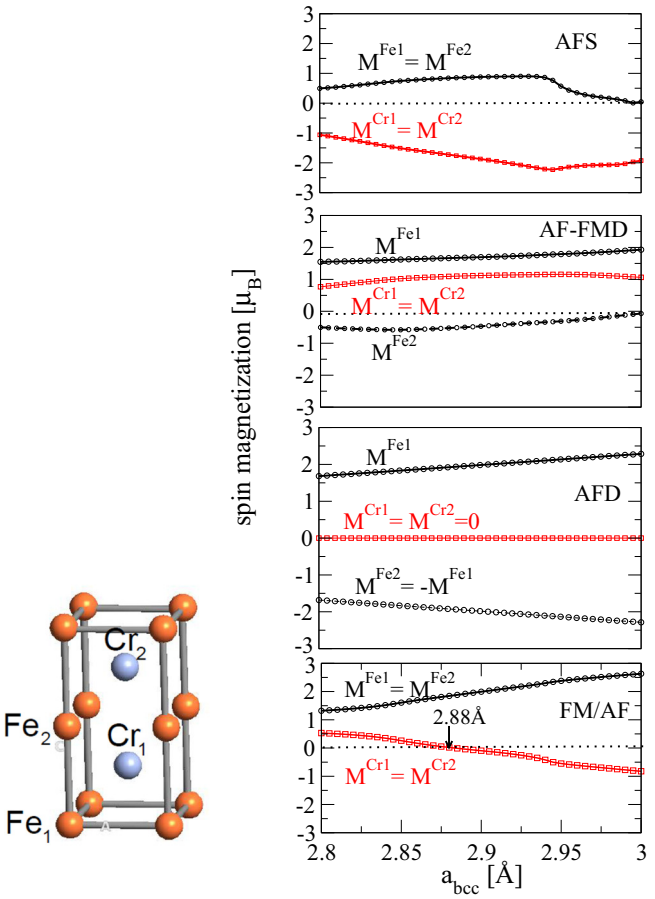

FIG. 7. Left: four-atom magnetic unit cell used for our TB calculations of the Fe-Cr B2 system. Right: local Fe and Cr moments versus the bcc lattice parameter a_{bcc} for the various magnetic phases. For the FM/AF phase, the magnetization of chromium is switching sign at 2.88 Å.

we show the evolution of the local moments decomposed on the four different atomic sites of the double unit cell for the four magnetic phases. And in Fig. 8 the corresponding total energy curves (per formula unit) are shown. The lowest-energy solution is the so-called FM/AF for which at the equilibrium distance (2.86 Å) both atoms have a positive magnetic moment below 2.88 Å, while above this threshold the magnetization of Cr becomes negative. The closest solution in energy is the AFD solution for which the chromium atoms have a zero magnetic moment, while iron atoms have large and opposite magnetizations. Just above in energy a rather unusual solution is obtained (AF-FMD) where both chromium atoms have the same positive magnetization while the two irons atoms have moments of opposite signs: a large and positive one and a small and negative one. The highest magnetic solution in energy is AFS where iron has a modest positive magnetization while chromium bears a large negative moment. Finally, the nonmagnetic solution is above all the magnetic ones showing that whatever the magnetic ordering, the system always gains energy by developing some kind of magnetism. We have checked our TB results on the relative stability of the various magnetic phases of the B2 structure by performing DFT-SIESTA calculations, the results of which are shown in Fig. 8. The agreement between TB and DFT is once again excellent. It is worth mentioning that the phase stability obtained from our TB model differs significantly from the one of Qiu *et al.* [52], but we believe that it is due to the functional that they have used (LSDA) rather than a failure of our model. Indeed, LSDA is known to overestimate bonding and consequently underestimate the lattice spacing which can strongly influence the phase stability of magnetic materials, in particular, in 3*d* transition metals.

We have also calculated the band structure and the projected density of states of Fe-Cr B2 in the FM/AF solution at the equilibrium lattice parameter $a = 2.86$ Å for which both magnetic moments of Fe and Cr are pointing in the same direction. Our TB results shown in Figs. 9 and 10 (left) are in very good agreement with the SIESTA calculations [Figs. 9 and 10 (right)], proving the predictive character of our TB model not only for the energetics and magnetization, but also for finer details of the electronic structure. Some of the differences between TB and SIESTA band structures can be attributed to the slight differences in the magnetization of

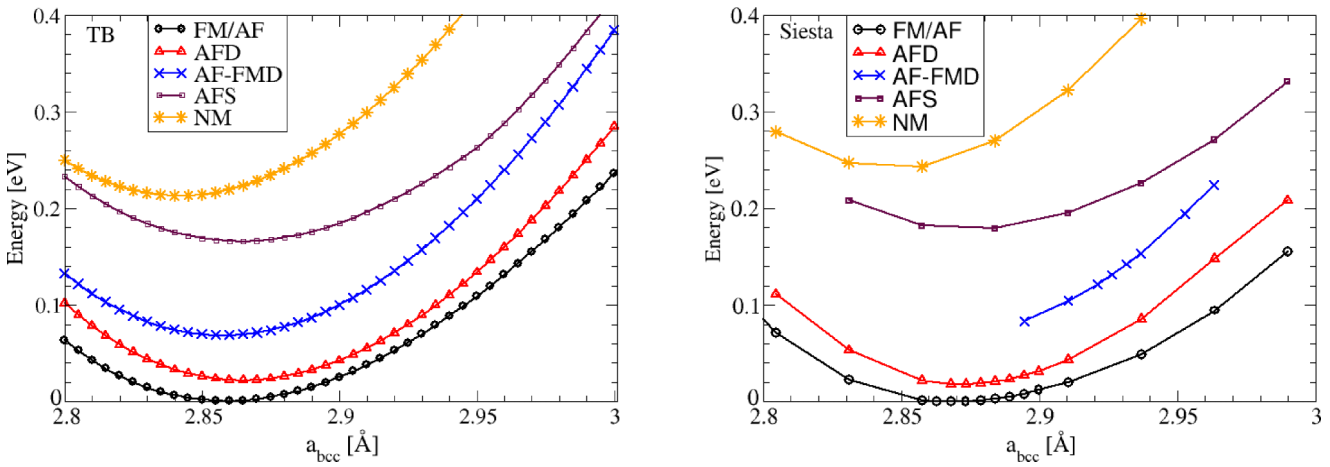

FIG. 8. Calculated (TB: left, SIESTA: right) total energies (per formula unit) versus the bcc lattice parameter a_{bcc} for the various magnetic phases. From SIESTA calculations the AF-FMD structure cannot be obtained for lattice parameters smaller than 2.89 Å. For better comparison, the minimum of the FM/AM curve has been set to zero in both calculations (TB and SIESTA).

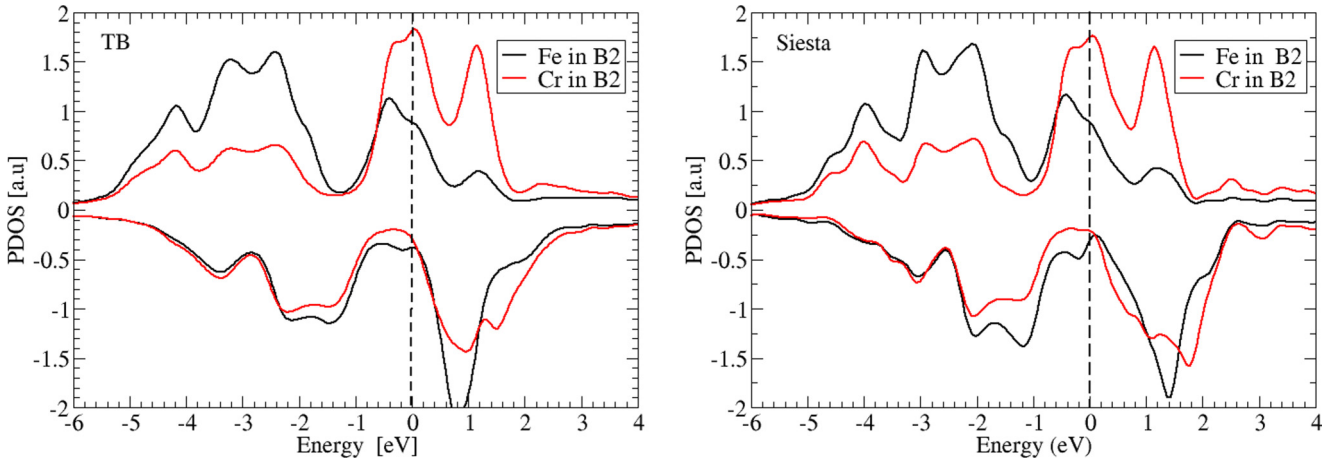

FIG. 9. Calculated (TB: left, SIESTA: right) spin-polarized density of states of states projected on the chromium (red line) and iron (black line) atomic orbitals for the Fe-Cr B2 FM/AF structure at the equilibrium lattice parameter 2.86 Å. Note that for this lattice constant, Fe and Cr both have positive magnetization.

Fe and Cr. We have also checked that the rescaling factor η almost does not affect the band structures and density of states, proving its minor role on the electronic properties.

D. Fe-Cr mixing enthalpies

The enthalpy of mixing for the binary Fe-Cr alloy is known to present a specific negative feature for low concentration of chromium while it becomes positive for larger Cr content [6]. An accurate prediction of this behavior is essential for studying any thermodynamic property of the alloy. We have calculated the mixing enthalpy $\Delta H(c)$ of bulk $Fe_{1-c}Cr_c$ by considering a $4 \times 4 \times 4$ supercell of bcc lattice containing 128 atoms in total and varying the concentration c of Cr from the lowest value $(1/128)$ to the highest value $(127/128)$. In all our calculations, we have adopted the Vegard's law and the lattice parameter of the alloy is then given by $a(c) = ca^{\mathrm{Cr}}_{\mathrm{bcc}} + (1-c)a^{\mathrm{Fe}}_{\mathrm{bcc}}$. Although slight deviations from this linear law have been reported in the literature [7], we have checked for a few concentrations around 10% (where the deviation is supposed to be the largest) that the equilibrium lattice constant is at most 0.1% larger than the one given by Vegard's rule, and the correction to the mixing enthalpy curve is marginal. We have considered the special quasirandom structures (sqs) which minimize the short-range order and are expected to be good representatives of solid solutions. $\Delta H(c)$ is evaluated by the standard formula

$$\Delta H\left(c = \frac{m}{n+m}\right) = \frac{E(\mathrm{Fe}_n\mathrm{Cr}_m) - nE(\mathrm{Fe}) - mE(\mathrm{Cr})}{n+m}, \tag{12}$$

where $E(\mathrm{Fe}_n\mathrm{Cr}_m)$ is the total energy of the supercell containing $n+m = 128$ atoms and $E(\mathrm{Fe})$, $E(\mathrm{Cr})$ are the equilibrium total energy per atom of bcc ferromagnetic Fe and bcc antiferromagnetic Cr. The results of our calculations are presented in Fig. 11 and compared to SIESTA calculations for the same set of structures. Our TB model reproduces very accurately the mixing-enthalpy curve from DFT-SIESTA over the whole range of concentration. In particular for the crossover between the region of negative and positive enthalpy the agreement is almost perfect. The curve presents a maximum for concentrations around 60% of chromium. It

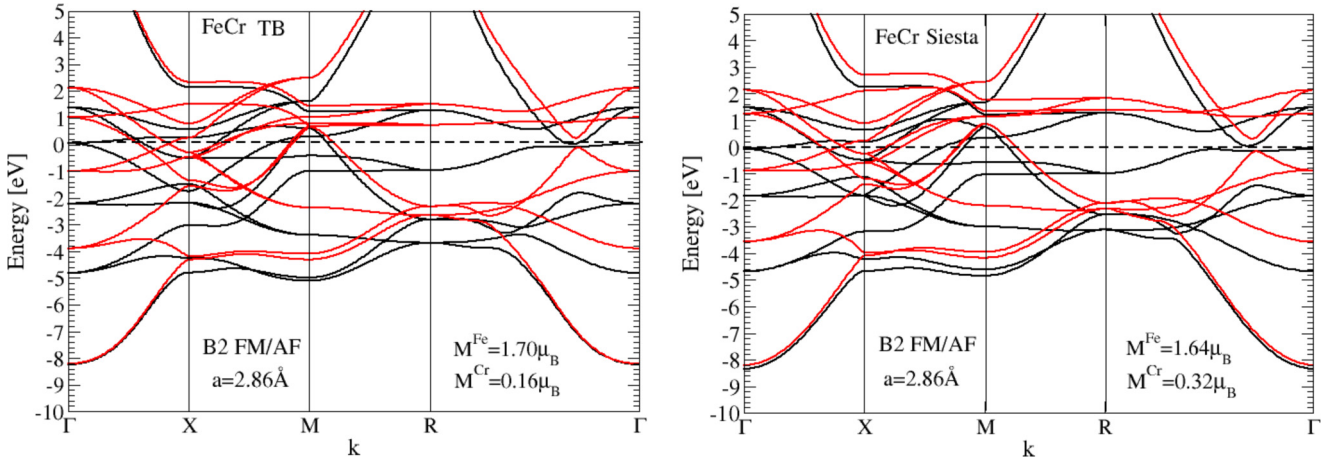

FIG. 10. Calculated (TB: left, SIESTA: right) spin-polarized band structure for the Fe-Cr B2 FM/AF structure at the equilibrium lattice parameter 2.86 Å. Note that for this lattice constant, Fe and Cr both have positive magnetization.

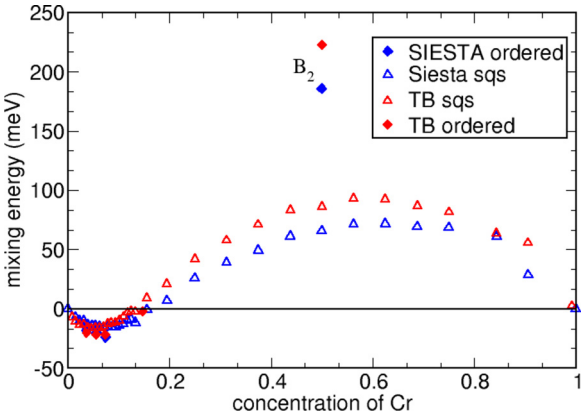

FIG. 11. Enthalpy of mixing as a function of the concentration c of Cr for the $Fe_{1-c}Cr_c$ alloy evaluated using our TB model compared to SIESTA results. For each concentration c we have used a sqs structure and only plotted the lowest-energy solution when several magnetic configurations were found (essentially in the high-concentration region). A few ordered structures were also calculated.

is also important to note that in the region rich in chromium, there often exist multiple magnetic solutions due to strong frustrations (typically when two Fe are first neighbors) so that we had to test several initial magnetizations and only the lowest in energy was retained. In addition, we have also considered the case of a few ordered structures essentially in the low-Cr concentration region, where, as expected, the mixing enthalpy of these structures is always slightly more negative than the one of the sqs structure at the same concentration. The tendency is reversed for larger concentrations, where the mixing enthalpy is positive. This can be illustrated by the "pathological" case of the B2 structure which in a sense maximizes the frustration and has the largest mixing enthalpy.

It is worth mentioning that the DFT-SIESTA and the TB predict a crossover Cr concentration of around 15%, other plane-wave DFT implementations using the PAW (projector augmented wave) method predict the crossover to occur around 7% of Cr [7,8,11], whereas the experimental value by Mirebeau *et al.* [5] is around 11%. The difference between the SIESTA and the plane-wave DFT is mainly due to the use of the type of norm-conserving pseudopotentials in SIESTA, which induces larger values of the magnetic moment on Cr in a dilute Fe-Cr alloy, and results in an overstabilization of the dilute alloys. Within the TB model, we note a sensitive dependence of the mixing curve and the crossover concentration on the rescaling parameter. Without any rescaling, the negative part even disappears and the whole enthalpy curve reaches much larger values (more than twice larger for the B2 phase). For $\eta = 1.023$, the crossover matches almost perfectly the one obtained by SIESTA but for intermediate values (between 1 and 1.023) the crossover will be shifted to lower concentrations.

E. Small Fe (Cr) clusters embedded in a Cr (Fe) matrix

Finally, a good description of embedded clusters is necessary for studying, for example, properties of precipitates in concentrated Fe-Cr alloys, where there is a tendency for phase separation (positive mixing enthalpy). Let us investigate two extreme cases: (i) small clusters of chromium in an iron FM bcc matrix and (ii) small clusters of iron in a chromium AF bcc matrix. Due to antagonistic magnetic interactions, we expect rather different behaviors in these two cases. Indeed, the magnetic interaction between two iron atoms is FM while it is AF between two chromium atoms or between an iron and a chromium atom at near-neighboring positions. We have considered four different clusters: a dimer, a triangular trimer, a tetrahedron, and a square tetramer embedded in a 4×4 supercell bcc latttice (the total number of atoms in the unit cell being 128). Note that since the lattice is body centered, the triangle and the tetrahedron are not regular since they connect either first or second neighbors. For each structure we have also investigated the possibility of occurrence of collinear and noncollinear magnetic configurations. In Tables III and IV, we have summarized the energetics and the magnetization for the

TABLE III. Mixing energies of various small Fe(Cr) clusters embedded in a Cr (Fe) matrix from TB collinear and noncollinear calculations. In the case of Cr clusters, noncollinear configurations do not exist while for Fe noncollinearity lowers the energy of the system. For a better comparison, we have also listed the difference of energy between a collinear and a noncollinear configuration for a unit cell of 128 atoms.

Cluster	$E_{\text{mix}}^{\text{col}}$ (meV/atom)	$E_{\text{mix}}^{\text{ncol}}$ (meV/atom)	$\Delta E_{\text{tot}}^{\text{col-ncol}}$ (meV/unit-cell)
Fe-Cr_{127}	2.4		0
Fe_2Cr_{126}	5.6	4.8	95
Fe_3Cr_{125} triangle	7.7	7.2	68
Fe_4Cr_{124} tetrahedron	10.7	8.7	250
Fe_4Cr_{124} square	14	13.8	47
$CrFe_{127}$	−7.2		0
Cr_2Fe_{126}	−7.2		0
Cr_3Fe_{125} triangle	−7.0		0
Cr_4Fe_{124} tetrahedron	−5.8		0
Cr_4Fe_{124} square	−10.5		0

TABLE IV. Magnetic moments for collinear and noncollinear magnetic coonfigurations of Fe(Cr) clusters embedded in a Cr(Fe) matrix. Whenever several atoms have the same magnetization, we have indicated its multiplicity (for example, ×4 in the case of the four equivalent Fe atoms forming a square). At the top of the table we have shown the four different noncollinear configurations obtained for the iron clusters.

Cluster	$m_{\text{Fe(Cr)}}^{\text{col}}$ (μ_B)	$m_{\text{Fe(Cr)}}^{\text{ncol}}$ (μ_B)	θ (degrees)
Fe-Cr_{127}	−1.17		
Fe_2Cr_{126}	0/-2.28	1.89×2	60/120
Fe_3Cr_{125} triangle	-2.17×2/-1.45	2×3	130×2/80
Fe_4Cr_{124} tetrahedron	-2.22×2/-1.28×2	2.08×4	120×2/60×2
Fe_4Cr_{124} square	2.15×4	2.07×4	45×4
$CrFe_{127}$	−2.3		
Cr_2Fe_{126}	-1.19×2		
Cr_3Fe_{125} triangle	-1.73×2/-1.26		
Cr_4Fe_{124} tetrahedron	-1.25×4		
Cr_4Fe_{124} square	-2×4		

TABLE V. Onsite TB parameters for Fe and Cr.

Element	Orbital	a	b	c	d	e
	s	0.0654	1.1144	11.4150	− 469.0171	7039.2378
Fe	p	0.3429	2.9992	− 12.7329	157.7794	− 880.7350
	d	0.0744	− 0.1788	1.6717	− 2.1260	26.77154
	s	0.0942	1.5564	5.1487	− 267.1346	6295.1471
Cr	p	0.3343	4.3267	− 21.3295	345.7256	− 2234.9309
	d	0.1135	− 0.3014	4.1017	− 21.2745	375.8615

eight structures to which we have added the results for a single atom.

First, let us note that no noncollinear configurations were found for these small Cr clusters. This is in agreement with previous DFT calculations which showed that noncollinearity only arises for slightly larger clusters [18]. In fact, a chromium atom does favor the surrounding of iron atoms rather than chromium ones: For instance, it is energetically more favorable (by about 0.4 eV) for two chromium atoms to be separated rather than first neighbors. A large part of this Cr-Fe interaction is due to magnetism which is reflected by the strong enhancement of the magnetic moment on a single chromium atom ($-2\mu_B$) in an iron matrix compared to its bulk value ($\pm 1\mu_B$), while in a dimer the magnetization of Cr drops to $-1.17\mu_B$. This is at the origin of the negative enthalpy of mixing for low-Cr concentration, indicating the tendency of Cr to make a solid solution.

As soon as a chromium atom is connected to other chromium atoms, the amplitude of its magnetic moment decreases rapidly. This is evidenced in the trimer where one Cr has two Cr atoms as first neighbors and the other two Cr have only one Cr as first neighbor (the other being second neighbor). The magnetic moment of the single Cr connected to two other Cr is almost the same as in bulk Cr, while the two others have a larger magnetization. The amplitude of magnetization of a Cr atom in tetrahedral geometry is almost the same as in the bulk, while in the case of a square-shaped cluster the Cr atoms are second neighbors and bear a large magnetic moment as large as in the case of an isolated Cr. Interestingly for all these clusters the magnetic order between Cr atom is ferromagnetic proving that the Fe-Cr AF interaction is dominating the system. The AF magnetic order between Cr atoms will only be recovered for larger clusters when a sufficiently large number of Cr atoms have a bulk environment [18].

In contrast, for each iron cluster a lower-energy noncollinear magnetic configuration does exist, in good agreement with DFT predictions [18]. In addition, in most cases several collinear solutions were found but it is always the FM one (among Fe atoms) that is the lowest in energy. This behavior can be attributed to a strong magnetic frustration which in fact does appear even for a single Fe atom in an AF Cr lattice since antiparallel coupling cannot be fulfilled for both first and second Fe-Cr neighbors. Contrary to the case of Cr in Fe, the magnetic moment of the single Fe atom surrounded by only Cr atoms is strongly decreased compared to its bulk value. We found a magnetization of around $1\mu_B$. In the case of the iron dimer in the collinear configuration an asymmetric solution is found where one atom has a zero magnetization while the other one is close to the iron bulk value. A symmetric solution is found in the noncollinear case where both iron atoms bear the same magnetic moment but canted with respect to one another (and to the Cr matrix). For the Fe trimer as in the case of Cr we found two Fe with large (negative) magnetization while the third Fe atom occupying the "up" sublattice of bcc-Cr has a lower (but still negative) magnetization. Similarly to the dimer in the noncollinear configuration, all the iron atoms bear the same large magnetic moment but canted with respect to one another. The iron tetrahedron is a very (magnetically) frustrated system as can be seen from the energy gain (250 meV) by relaxing the collinear constraint to a noncollinear configuration. In contrast, the square is a much less frustrated system but its mixing energy is higher since chemically iron prefers to form bonds with iron rather than with chromium.

TABLE VI. Slater-Koster hopping TB parameters for Fe and Cr.

	Fe				Cr			
Hopping	p	f	g	h	p	f	g	h
$ss\sigma$	0.0129	−0.7417	0.0392	0.8020	0.3528	−0.6590	0.0452	0.7572
$sp\sigma$	−12.7214	3.7405	0.0304	0.9093	−10.9485	2.8407	0.0836	0.9036
$pp\sigma$	−6.9952	2.4422	−0.1802	0.7387	−8.3294	2.6866	−0.1647	0.7467
$pp\pi$	148.7768	−258.4013	0.000	4.4487	734.5209	−98.8765	0.0000	4.1281
$sd\sigma$	2.2094	−0.8765	0.0051	0.8878	3.6878	−1.2032	0.028	0.8847
$pd\sigma$	2.5908	−1.0730	0.0589	0.8201	7.7230	−2.1013	−0.0054	0.9012
$pd\pi$	−35.8525	11.8431	−0.2706	1.1397	−131.0844	39.6150	−0.8188	1.2228
$dd\sigma$	−1.8022	0.3038	−0.0164	0.7747	−2.4171	0.3028	−0.0221	0.8357
$dd\pi$	6.6544	−1.5783	0.1439	0.9635	5.6299	−0.9789	0.0713	0.9314
$dd\delta$	−0.0622	−0.5314	−0.0063	1.1286	14.0914	−6.7593	−0.0344	1.2717

TABLE VII. Slater-Koster overlap TB parameters for Fe and Cr.

	Fe				Cr			
Overlap	p	f	g	h	p	f	g	h
$ss\sigma$	2.0429	−0.4161	0.2115	0.8615	2.6878	−0.28736	0.1877	0.8581
$sp\sigma$	0.6079	−0.4843	−0.0103	0.7465	2.4309	−1.6073	0.0026	0.8052
$pp\sigma$	3.8114	−1.3166	−0.0014	0.7151	4.4633	−1.5723	−0.0047	0.7554
$pp\pi$	−0.2540	1.9711	−0.0214	0.8594	−5.6357	2.7262	0.0072	0.8954
$sd\sigma$	168.04884	−25.9315	−2.4944	1.2560	3.74415	−0.7553	0.1202	0.9730
$pd\sigma$	0.2049	−0.2692	0.0348	0.6915	0.36665	−0.0816	0.0099	0.6860
$pd\pi$	−0.5420	0.0992	−0.0046	0.4195	−0.6352	−0.2187	−0.0012	0.8107
$dd\sigma$	22.7769	−1.2565	−0.4900	1.1789	−0.90857	0.8767	−0.0911	0.8521
$dd\pi$	3.6198	−1.5098	−0.4374	1.2132	−2.0957	0.2115	−0.0017	0.8834
$dd\delta$	10.2436	−0.5319	−0.1977	1.1980	0.2764	−0.0260	−0.0001	0.7488

IV. CONCLUSIONS

We have developed a *spd* TB model for the Fe-Cr system. The magnetism is treated within the Stoner formalism, beyond the usual collinear approximation. A major advantage of this model consists in a rather simple fitting procedure. In particular, no specific property of the binary system is explicitly required in the fitting database. Starting from the parameters of the pure systems, the hopping and the overlap integrals for the heteroelement (Fe-Cr) pairs are simply obtained by an arithmetic average multiplied by a unique rescaling factor.

The resulting TB model is proved to be accurate and highly transferable for electronic, magnetic, and energetic properties of a large variety of structural and chemical environments: surfaces, interfaces, embedded clusters, and the whole compositional range of the binary alloy. Note that none of these properties have been included in the fitting data.

It is worth mentioning that the present TB approach can apply to other binary magnetic transition-metal alloys. It is, however, particulary suitable for systems such as the Fe-Cr. Due to a very small size difference between Fe and Cr, for instance in a bcc phase, several energetic properties of the alloy come to be driven by the electronic and magnetic interactions. The present TB model is also very promising if coupled with kinetic Monte Carlo simulations, for investigating finite-temperature magnetic and microstructural evolution in Fe-Cr alloys, where large-scale simulations are required.

ACKNOWLEDGMENT

This work was performed using computer resources from GENCI-DARI (Grant No. x2016096020), and IFERC-CSC Helios supercomputer within the SISteel project.

APPENDIX: TB PARAMETERS

In Table V are listed the numerical values of the TB parameters to obtain the onsite elements of the Hamiltonian given by Eqs. (2) and (3) in which the distances are expressed in bohrs and the energies in Rydbergs. The Λ parameter [Eq. (3)] is taken equal to 1.3 for both elements.

In Tables VI and VII are listed the numerical values of the TB parameters to obtain the Slater-Koster hopping and overlap integrals of the Hamiltonian given by Eq. (4) in which the distances are expressed in bohrs and energies in Rydbergs. The heteronuclear (Fe-Cr) hopping (and overlap) integrals are taken as the arithmetic average multiplied by the rescaling factor $\eta_{\text{Fe-Cr}} = 1.023$ [see Eq. (9)].

[1] R. Soulairol, C.-C. Fu, and C. Barreteau, Phys. Rev. B **84**, 155402 (2011).
[2] M. Y. Lavrentiev, R. Soulairol, C.-C. Fu, D. Nguyen-Manh, and S. L. Dudarev, Phys. Rev. B **84**, 144203 (2011).
[3] M. Hennion, J. Phys. F: Met. Phys. **13**, 2351 (1983).
[4] I. Mirebeau, M. Hennion, and G. Parette, Phys. Rev. Lett. **53**, 687 (1984).
[5] I. Mirebeau and G. Parette, Phys. Rev. B **82**, 104203 (2010).
[6] P. Olsson, I. Abrikosov, L. Vitos, and J. Wallenius, J. Nucl. Mater. **321**, 84 (2003).
[7] P. Olsson, I. A. Abrikosov, and J. Wallenius, Phys. Rev. B **73**, 104416 (2006).
[8] T. P. C. Klaver, R. Drautz, and M. W. Finnis, Phys. Rev. B **74**, 094435 (2006).
[9] A. Kissavos, S. Simak, P. Olsson, L. Vitos, and I. Abrikosov, Comput. Mater. Sci. **35**, 1 (2006).
[10] P. A. Korzhavyi, A. V. Ruban, J. Odqvist, J.-O. Nilsson, and B. Johansson, Phys. Rev. B **79**, 054202 (2009).
[11] M. Levesque, E. Martínez, C.-C. Fu, M. Nastar, and F. Soisson, Phys. Rev. B **84**, 184205 (2011).
[12] P. Grünberg, R. Schreiber, Y. Pang, M. B. Brodsky, and H. Sowers, Phys. Rev. Lett. **57**, 2442 (1986).
[13] M. N. Baibich, J. M. Broto, A. Fert, F. Nguyen Van Dau, F. Petroff, P. Etienne, G. Creuzet, A Friederich, and J. Chazelas, Phys. Rev. Lett. **61**, 2472 (1988).
[14] G. J. Ackland, Phys. Rev. Lett. **97**, 015502 (2006).
[15] A. V. Ruban, P. A. Korzhavyi, and B. Johansson, Phys. Rev. B **77**, 094436 (2008).
[16] M. Ropo, K. Kokko, E. Airiskallio, M. P. J. Punkkinen, S. Hogmark, J. Kollar, B. Johansson, and L. Vitos, J. Phys.: Condens. Matter **23**, 265004 (2011).
[17] P. Olsson, C. Domain, and J. Wallenius, Phys. Rev. B **75**, 014110 (2007).

[18] C.-C. Fu, M. Y. Lavrentiev, R. Soulairol, S. L. Dudarev, and D. Nguyen-Manh, Phys. Rev. B **91**, 094430 (2015).
[19] H. Yamamoto, Jpn. J. Appl. Phys. **3**, 745 (1964).
[20] E. Martínez, O. Senninger, C.-C. Fu, and F. Soisson, Phys. Rev. B **86**, 224109 (2012).
[21] O. Senninger, E. Martínez, F. Soisson, M. Nastar, and Y. Bréchet, Acta Mater. **73**, 97 (2014).
[22] P. Olsson, J. Wallenius, C. Domain, K. Nordlund, and L. Malerba, Phys. Rev. B **72**, 214119 (2005).
[23] A. Caro, D. A. Crowson, and M. Caro, Phys. Rev. Lett. **95**, 075702 (2005).
[24] E. del Rio, J. M. Sampedro, H. Dogo, M. J. Caturla, M. Caro, A. Caro, and J. M. Perlado, J. Nucl. Mater. **408**, 18 (2011).
[25] D. Stoeffler and F. Gautier, J. Magn. Magn. Mater. **147**, 260 (1995).
[26] E. Martinez, R. Robles, D. Stoeffler, and A. Vega, Phys. Rev. B **74**, 184435 (2006).
[27] R. Robles, E. Martinez, D. Stoeffler, and A. Vega, Phys. Rev. B **68**, 094413 (2003).
[28] D. Stoeffler and C. Cornea, J. Magn. Magn. Mater. **240**, 223 (2002).
[29] A. T. Paxton and M. W. Finnis, Phys. Rev. B **77**, 024428 (2008).
[30] D. Nguyen-Manh and S. L. Dudarev, Phys. Rev. B **80**, 104440 (2009).
[31] E. J. McEniry, G. K. H. Madsen, J. F. Drain, and R. Drautz, J. Phys.: Condens. Matter **23**, 276004 (2011).
[32] C. Barreteau, R. Guirado-López, D. Spanjaard, M. C. Desjonquères, and A. M. Oleś, Phys. Rev. B **61**, 7781 (2000).
[33] G. Autès, C. Barreteau, D. Spanjaard, and M.-C. Desjonquères, J. Phys.: Condens. Matter **18**, 6785 (2006).
[34] C. Barreteau, D. Spanjaard, and M.-C. Desjonquères, C. R. Phys. **17**, 406 (2016).
[35] M. J. Mehl and D. A. Papaconstantopoulos, Phys. Rev. B **54**, 4519 (1996).
[36] J. C. Slater and G. F. Koster, Phys. Rev. **94**, 1498 (1954).
[37] C. Barreteau and D. Spanjaard, J. Phys.: Condens. Matter **24**, 406004 (2012).
[38] J. F. Janak, Phys. Rev. B **16**, 255 (1977).
[39] R. Soulairol, C.-C. Fu, and C. Barreteau, J. Phys.: Condens. Matter **22**, 295502 (2010).
[40] R. Iglesias and S. Palacios, Acta Mater. **55**, 5123 (2007).
[41] P. Turchi and F. Ducastelle, *The Recursion Method and Its Applications*, Vol. 58 of Springer Series in Solid-State Sciences (Springer, Berlin, 1987).
[42] D. Li, A. Smogunov, C. Barreteau, F. Ducastelle, and D. Spanjaard, Phys. Rev. B **88**, 214413 (2013).
[43] D. Li, C. Barreteau, M. R. Castell, F. Silly, and A. Smogunov, Phys. Rev. B **90**, 205409 (2014).
[44] J. Soler, E. Artacho, J. Gale, A. Garcia, J. Junquera, P. Ordejón, and D. Sanchez-Portal, J. Phys.: Condens. Matter **14**, 2745 (2002).
[45] P. Błoński and A. Kiejna, Surf. Sci. **601**, 123 (2007).
[46] T. Ossowski and A. Kiejna, Surf. Sci. **602**, 517 (2008).
[47] M. Punkkinen, Q.-M. Hu, S. Kwon, B. Johansson, J. Kollar, and L. Vitos, Philos. Mag. **91**, 3627 (2011).
[48] M. Aldén, H. L. Skriver, S. Mirbt, and B. Johansson, Phys. Rev. Lett. **69**, 2296 (1992).
[49] M. P. J. Punkkinen, S. K. Kwon, J. Kollár, B. Johansson, and L. Vitos, Phys. Rev. Lett. **106**, 057202 (2011).
[50] S. Lu, Q.-M. Hu, R. Yang, B. Johansson, and L. Vitos, Phys. Rev. B **82**, 195103 (2010).
[51] D. F. Johnson, D. Jiang, and E. A. Carter, Surf. Sci. **601**, 699 (2007).
[52] S. L. Qiu, P. M. Marcus, and V. L. Moruzzi, J. Appl. Phys. **85**, 4839 (1999).